Nonlinear dynamics of beta-induced Alfvén eigenmode in tokamak

H. S. Zhang,[1,2] Z. Lin,[2,a] W. Deng,[2] I. Holod,[2] Z. X. Wang,[2] Y. Xiao,[3] and W. L. Zhang[4]

[1]*Fusion Simulation Center, Peking University, Beijing 100871, China*
[2]*Department of Physics and Astronomy, University of California, Irvine, California 92697, USA*
[3]*Institute for Fusion Theory and Simulation, Zhejiang University, Hangzhou 310027, China*
[4]*CAS Key Laboratory of Plasma Physics, University of Science and Technology of China, Hefei, Anhui 230026, China*

The beta-induced Alfvén eigenmode (BAE) excited by energetic particles in toroidal plasmas is studied in the global gyrokinetic simulations. It is found that the nonlinear BAE dynamics depends on the deviation from the marginality. In the strongly driven case, the mode exhibits a bursting state with fast and repetitive chirping. The nonlinear saturation is determined by the thermal ion nonlinearity and has no clear dependence on the linear growth rate. In the weakly driven case, the mode reaches a nearly steady state with small frequency chirping. The nonlinear dynamics is dominated by the energetic particle nonlinearity. In both cases, the nonlinear intensity oscillation and frequency chirping are correlated with the evolution of the coherent structures in the energetic particle phase space. Due to the radial variation of the mode amplitude and the radially asymmetric guiding center dynamics, the wave-particle interaction in the toroidal geometry is much more complex than the conventional one-dimensional wave-particle interaction paradigm. © 2013 American Institute of Physics. [http://dx.doi.org/10.1063/1.4776698]

I. INTRODUCTION

The β-induced Alfvén eigenmode (BAE)[1–4] observed in tokamak experiments can be destabilized by energetic particles and, in return, cause the loss of the energetic particles. The BAE oscillates with the geodesic acoustic mode (GAM) frequency,[5–7] which is on the order of the thermal ion transit frequency. Therefore, BAE has strong resonant interactions with both thermal ions and energetic particles. The BAE excitation by ion cyclotron resonance heating (ICRH) is observed in Tore-Supra[8,9] and ASDEX Upgrade.[10,11] The BAE excitation by ECRH and magnetic island are also observed in HL-2A.[12,13] In these experiments, the BAE frequency sweeping phenomenon is found before the sawtooth crash, which is mainly due to the change of the equilibrium. Meanwhile, fast frequency chirping of various Alfvén waves is widely observed in tokamak experiments. The frequency chirping of the toroidal induced Alfvén eigen mode (TAE) and energetic particle mode (EPM) are found in D-IIID,[14] NSTX,[15,16] JT-60U,[17] JET,[18] START, and MAST.[19] The low frequency waves, such as fishbone and BAE, also exhibit fast frequency chirping.[20,21] Particularly, the transition from the downward chirping bursting state to the nearly steady state of the nonlinear BAE is observed in recent experiment in ASDEX.[21,22] The enhancement of the energetic particle transport is also observed during the fast chirping events,[15,16] which suggest that the fast chirping of the Alfvén eigenmodes is more relevant to the energetic particle transport than the steady state of the Alfvén eigenmodes.

The BAE dispersion relation and excitation have also been studied theoretically. Kinetic theory shows that the BAE continuum accumulation point has a slight downshift and is related to diamagnetic effects, elongation, and the trapped particles.[23] The BAE damping effect is investigated through numerical solution.[24] The relation between BAE and GAM has also been discussed.[6,25,26] The BAE excitation threshold is calculated theoretically, which is in agreement with the experiments.[27] Regarding the nonlinear physics, it is also shown that the purely nonlinear BAE steady-state regimes are possible for Tore-Supra parameters.[28] The one-dimensional bump-on-tail model or Berk-Breizman model with source and sink has been applied to explain many kinds of Alfvén wave frequency chirping.[29,30] By perturbatively treating the energetic particles, the model reproduces the nonlinear up-and-down frequency chirping phenomenon and the spontaneous formation of the hole-and-clump pair in the phase space.[30–32] The improved model with a nonperturbative treatment of the beam exhibits a strong asymmetry frequency chirping, and the chirping is linearly dependent on time.[33] The extended model with dynamical friction and velocity space diffusion has been developed to study the evolution of frequency chirping and hole-and-clump formation.[34]

The fully self-consistent three-dimensional simulations have also been applied to study the Alfvén waves and the frequency chirping in tokamaks. The HAGIS code recovers the self-consistent up-and-down frequency chirping of marginally unstable TAEs.[35] The M3D simulation shows that the nonlinear fishbone saturates along with downward frequency chirping.[36] Both of the simulations are carried out without sources and sinks. The M3D simulation with source and sink also shows that the nonlinear TAE exhibits oscillatory behavior with up-and-down frequency chirping.[37] These simulations successfully reproduce a single burst of the chirping. The repetitive chirping and bursting state observed

[a]Author to whom correspondence should be addressed. Electronic mail: zhihongl@uci.edu.

in experiments has not been well explained. Furthermore, the flattening of the particle distribution function near the resonance region is often observed after the nonlinear saturation. This flattening is believed to be very important to the nonlinear mode saturation and can be induced through nonlinear wave-particle trapping or the radial transport of resonant particles. The later one is often associated with the radial convection of the mode amplitude, which can also result in the frequency chirping such as the EPMs.[38] Therefore, it is essential to identify whether the frequency chirping is due to the nonlinear particle dynamics itself or the profile flattening. On the other hand, few works have been reported on BAE simulations.[39,40]

Gyrokinetic toroidal code (GTC)[41] has been successfully applied to the gyrokinetic simulation of TAE,[42,43] RSAE,[44–46] and GAM.[47,48] The GTC simulation of the BAE linear excitation has been reported.[49] Recently, the fast and repetitive frequency chirping of the BAE is observed by the massively parallel GTC simulation without sources and sinks in a realistic toroidal geometry.[50] In this work, we mainly focus on the nonlinear BAE dynamics and its dependence on the deviation from the marginality. The current simulations find that the BAE saturation amplitude is linearly dependent on the square of the linear growth rate near marginality, which is consistent with the picture of nonlinear saturation via phase space trapping.[29] When the BAE is well deviated from the marginality, the saturation amplitude has no clear dependence on the linear growth rate because the phase space island size is comparable to the radial mode width. We further find that in the strongly driven case, the BAE exhibits a bursting state with fast, repetitive, and mostly downward chirping. The chirping has a period of sub-millisecond and a 90° phase shift from the amplitude oscillation. The nonlinear saturation is mainly determined by the thermal ion nonlinearity. The fast and repetitive chirping is correlated with the evolution of the energetic particle phase space structures. In the weakly driven case, the BAE exhibits a nearly steady state with small frequency chirping. The saturation amplitude and the nonlinear evolution are dominated by the energetic particle nonlinearity.

The comparison of the phase space structures between the nonlinear BAE and the one-dimensional nonlinear Landau damping shows that the wave-particle interaction in the toroidal geometry is much more complex than the conventional one-dimensional wave-particle interaction paradigm. When the radial width of the energetic particle phase space islands is as large as the radial mode width in the strongly driven case, the nonlinear BAE dynamics can be strongly affected by the radial variations of mode amplitude and the radially asymmetric guiding center dynamics in the toroidal geometry.

The paper is organized as follows: The deviation from the BAE marginality is discussed in Sec. II. The nonlinear evolution of the strongly driven and weakly driven BAE is presented in Secs. III and IV, respectively. In Sec. V, comparisons of the phase space between the BAE simulations and one-dimensional nonlinear Landau damping are discussed. Section IV is the conclusion.

II. DEPENDENCE OF BAE NONLINEAR DYNAMICS ON THE DEVIATION FROM MARGINALITY

The BAE linear excitation properties and GTC benchmarks with XHMGC were reported in our previous work.[49] In the current study, we focus on the BAE nonlinear dynamics. The BAE is excited in a tokamak with concentric flux-surfaces. In our simulation, the radius profile of safety factor q is $q = 1.797 + 0.8(\psi/\psi_w) - 0.2(\psi/\psi_w)^2$, where ψ is the poloidal flux function with $\psi(r=0) = 0, \psi(r=a) = \psi_w$, and $a = 0.328R_0$ is the minor radius at the wall. The $q = 2$ rational surface is located at a minor radius $r_0 = 0.164R_0$ (Fig. 1(a)), where R_0 is the major radius. The electron density n_0 is uniform and the energetic particle (EP) density profile is $n_h = 0.01n_0 * (1.0 + 0.35 * (\tanh((0.26 - \psi/\psi_w)/0.06) - 1.0))$, so that the EP density gradient has a maximum value of R_0/L_n near $q = 2$ surface, where L_n is the EP density gradient scale length (Fig. 1(b)). Both thermal and energetic ions are protons with a Maxwellian velocity distribution and are treated using the nonlinear gyrokinetic equations,[51] while electrons are treated as a massless fluid.[52] The temperature is uniform for all species with $T_e = 0$ and $T_h = 25T_i$. The thermal plasma beta at r_0 is $\beta = 8\pi n_0 T_i/B_0^2 = 0.0072$ with B_0 being the on-axis magnetic field. Without losing generality, the simulation treats a single toroidal mode number $n = 3$, which has $k_\theta \rho_i = 0.044$ for $R_0 = 838\rho_i$. Here, k_θ is the poloidal wavevector and ρ_i the thermal ion gyroradius. In our gyrokinetic simulation, both EP and thermal ion nonlinearities are retained, while the coupling between different n modes is ignored due to lack of resonance condition between different n modes. The generation of the zonal fields will be studied in future work. Since $k_\parallel \sim 0$ for BAE, a filter is applied to keep only the $m \in [nq - 2, nq + 2]$ poloidal harmonics to avoid the high $k_\parallel$ noise. A slow sound approximation is used to suppress the ion acoustic wave (i.e., $E_\parallel = 0$). All perturbed quantities are set to be zero at the radial boundaries $(r/R_0 = 0.048, 0.24)$. Numerical convergence with
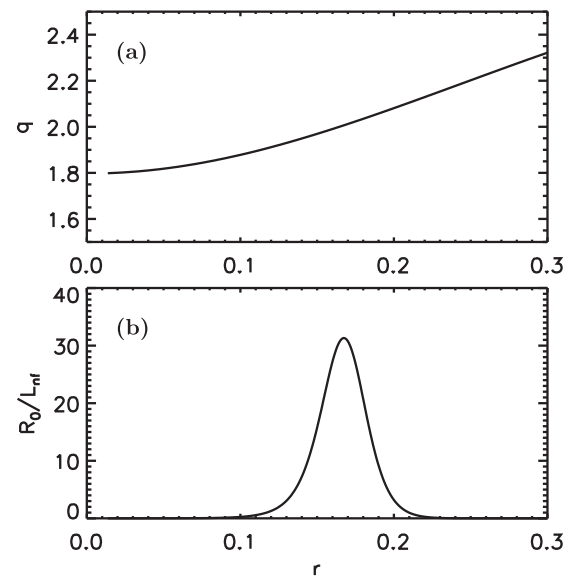

FIG. 1. q profile (a) and R/L_{nf} profile (b) in radial direction.

respect to number of particles, spatial grid size, and time step has been achieved.

By changing the EP density gradient, the linear growth rate of BAE is adjusted and a series of GTC simulations have been performed to scan the deviation from marginality. Figure 2 shows that the BAE saturation amplitude is proportional to the square of the linear growth rate when (γ/ω_0) < 0.05, which is located in the marginal region. However, there is no strong dependence of the amplitude on the growth rate when $(\gamma/\omega_0) > 0.07$, which is well deviated from the marginality and is more relevant for transport. Therefore, the nonlinear BAE simulation can be divided into the weakly driven $((\gamma/\omega_0) < 0.05)$ and strongly driven cases $((\gamma/\omega_0) > 0.07)$. We further find that the BAE saturation mechanism and nonlinear behavior are quite different between the strongly driven and weakly driven cases, which we will discuss in Secs. III and IV, respectively. Furthermore, the linear dependence of $e\delta\phi/T_i$ on $(\gamma/\omega_0)^2$ suggests that the nonlinear saturation may be due to the nonlinear wave-particle trapping paradigm like the one-dimensional nonlinear Landau damping problem.[53] But due to the toroidal geometry and non-uniform radial mode amplitude, the saturation mechanism is much more complex than the 1D problem, which we will discuss in Sec. V.

III. STRONGLY DRIVEN BAE

In the strongly driven BAE simulation, we set the maximum EP gradient to be $R_0/L_n = 31$ (Fig. 1(b)) and drive the BAE with a small initial amplitude noise. The BAE mode structure forms around the mode rational surface r_0, and the amplitude grows with a real frequency $\omega_{BAE} = 0.96\omega_0$ and a growth rate $\gamma = 0.09\omega_0$, which suggests that it is well deviated from the marginality. Here, $\omega_0 = \sqrt{(7T_i/2 + 2T_e)/(m_i R_0^2)}$ is the geodesic acoustic mode frequency[5] with m_i being the proton mass. The mode amplitude exhibits a nonlinear oscillation bursting state with a period of about ten wave periods (red curve in Fig. 1(a) of Ref. 50), i.e., less than one millisecond for typical experimental parameters. We further analyze the BAE frequency spectrum by applying the wavelet transform to the real part of $\delta\phi$ (Fig. 1(b) of Ref. 50) and the time evolution of the wavelet power spectrum exhibits a regular oscillation of wave frequency ω, dominated by mostly downward chirping. The frequency with the highest power intensity (black curve in Fig. 1(a) of Ref. 50) shows that the amplitude
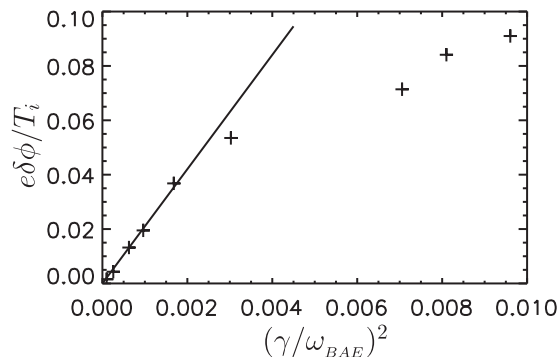
oscillation has roughly a $90°$ phase lag behind the frequency oscillation. Since the mode amplitude is relatively low during the upward chirping, experimental measurements will mostly see the downward chirping. All of these features from our simulations have recently being observed in the TAE mode in NSTX experiment[15,16] and BAE mode in ASDEX experiment,[21,22] suggesting a universal mechanism underlying the chirping dynamics. More detailed information can be found in the Ref. 50.

The fast oscillations of wave frequency and amplitude persist without external sources and sinks to replenish the EP distribution function, and the EP density gradient changes little after the mode saturation, suggesting the important roles of nonlinear wave and particle dynamics. In our simulations, both the thermal ions and EPs are governed by the nonlinear gyrokinetic equations. To delineate the nonlinearity of thermal and energetic ions, two controlled simulations are performed. One simulation is performed with nonlinear thermal ions and linear EPs (red lines in Fig. 3), the other is carried out with linear thermal ions and nonlinear EPs (black lines in Fig. 3). The simulation with nonlinear thermal ions and linear EPs has similar saturation amplitude to the simulation with both nonlinearities (green lines in Fig. 3), but no oscillations of frequency and amplitude are observed, while the simulation with linear thermal ions and nonlinear EPs saturates at the amplitude three times higher and some oscillations of frequency and amplitude are observed. Therefore, the thermal ion nonlinearity is responsible for the BAE saturation and the initial frequency downshift, while the energetic ion nonlinearity is responsible for the frequency oscillation for current simulation parameters. The investigation of the nonlinear BAE mode structure (Fig. 2 of Ref. 50) further indicates that the thermal ions cannot be simply represented as a linear damping rate when describing the nonlinear BAE dynamics. The frequency downshift and the suppression of the saturation amplitude are also observed in recent nonlinear TAE simulation with nonlinear MHD effect.[54] The effect of thermal ion nonlinearity needs more investigation.

We now examine linear and nonlinear interactions between EP and BAE to elucidate the frequency oscillation mechanism. The resonance condition[56] for a low-frequency

FIG. 2. The saturation amplitude $e\delta\phi/T_i$ vs square of the linear growth rate γ.
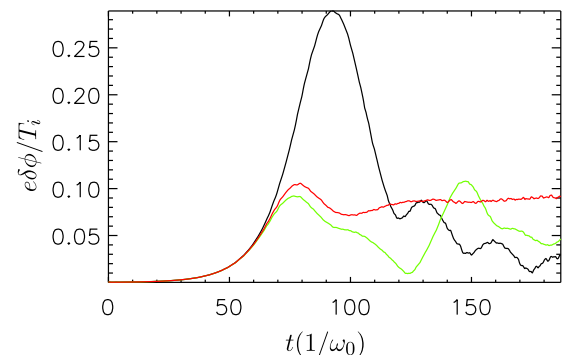

FIG. 3. Controlled simulations for strongly driven cases. Black line is the simulation with linear thermal ions and nonlinear EPs. Red line is the simulations with nonlinear thermal ions and linear EPs. Green line is the simulations with both nonlinearity.

wave in a general axisymmetric system is $\omega - k_\parallel v_\parallel - p\omega_t = 0$ for passing particles, and $\omega - n\omega_{pre} - p\omega_b = 0$ for trapped particles. Here, p is an integer number, $\omega_t, \omega_b, \omega_{pre}$ are guiding center transit, bounce, and precessional frequencies,[57] respectively. The resonances induce locally large fluctuations of the perturbed distribution function δf_h in the phase space. The relative strength of resonances can be inferred from the intensity of the EP entropy δf_h^2.[48] Figure 4 shows the linear and nonlinear EP entropy δf_h^2 as a function of the equilibrium constants of motion (E, λ). Here, E is the guiding center kinetic energy and $\lambda = \mu B_0/E$ is a pitch angle parameter with μ the magnetic moment. The trapped-passing boundary at r_0 is $\lambda = 1 - r_0/R_0$. Four resonances can be identified in both linear and nonlinear stages (Figs. 4(a) and 4(b)). The most prominent resonance is the precessional resonance ($\omega = \omega_d \equiv n\omega_{pre}$) of deeply trapped particles. The others include the drift-bounce resonance ($\omega = \omega_d + p\omega_b$) and the second harmonic resonance ($\omega = 2\omega_d$) of trapped particles, and the transit resonance ($\omega = \omega_t$) of passing particles. From linear to nonlinear stage, all resonance regions move to the lower E while the change in λ is much smaller. Variations of the resonance energy and radial excursions of resonant particles can modify ω_d and induce the wave

frequency chirping. The dominant radial excursions are associated with the nonlinear particle trapping as indicated by island-like structures of δf_h at the nonlinear stage with pairs of positive and negative density perturbations (Fig. 4(c)).

Since the precessional resonance is the dominant resonance for the excitation of BAE, we will mainly focus on the interaction between EP and BAE by precessional resonance in the following investigation. The dynamics of the precessional resonance can be simply described by a radially local 1D model using canonical variables (ζ, ω_d) with ζ the toroidal angle. The evolution of $\delta f_h/f_{h0}$ in the (ζ, ω_d) phase space for the strongly driven simulation is shown in Fig. 3 of Ref. 50, which shows that the frequency chirping is consistent with the evolution of coherent structures in the (ζ, ω_d) phase space for precessional resonance, which propagate at the local ω_d. The contribution of other sideband resonances to the evolution of the coherent structures, and the frequency chirping is subdominant. The $\omega_d(E, r)$ variations come from the changes in the kinetic energy E and the radial r excursions of resonant particles. The phase space coherent structures and the oscillations of the mode amplitude both indicate the onset of the nonlinear trapping of resonant particles.[58] However, the trapped particle dynamics in the current simulations is much more complex due to radial variations of mode amplitude and radially asymmetric particle dynamics in the toroidal geometry.

For the precessional resonance that preserves the magnetic moment and the longitudinal invariant in an axisymmetric toroidal system, the nonlinear dynamics of guiding centers can be completely described by a pair of action-angle variables (ζ, P_ζ) with $P_\zeta = g\rho_\parallel - \psi$ the canonical angular momentum, $2\pi g$ the poloidal current, $\rho_\parallel = v_\parallel/B$ the normalized parallel velocity, and ψ the poloidal flux function labeling the radial position r.[57] By tracking the nonlinear orbits of deeply trapped particles, the structure of the EP distribution function in the (ζ, P_ζ) space are examined in Fig. 4 of Ref. 50. We found that the nonlinear wave-particle trapping structures are formed at the beginning of the saturation. The P_ζ variations of the coherent structures can easily induce the wave frequency chirping range of $\approx 15\%$. However, due to the asymmetry of ω_d in radial direction, the evolution of the mode structure and the onset of the nonlinear wave-particle trapping are not radially symmetric. Meanwhile, the width of the phase space islands is found to be comparable to the radial mode width. Therefore, the radial variations of the mode amplitude are important to the nonlinear dynamics of resonant particles. The resonant particles away from the mode rational surface experience weaker $E \times B$ radial convection and are dominated by free streaming with their local velocity ω_d. The islands are stretched and destroyed through the free streaming process when the nonlinear BAE amplitude decreases. The associated linear phase-mixing effect is further enhanced by the dependence of the ω_d variation rate $(d\omega_d/d\psi)$ on the magnetic moment and the longitudinal invariant. The destruction of the islands allows BAE to grow again. The cycle of the formation and destruction of coherent structures in the phase space thus persists without sources and sinks. The time it takes for an island to stretch in the ζ direction over a distance of the wavelength is the linear phase-mixing time, which defines the life time of the coherent structures and the
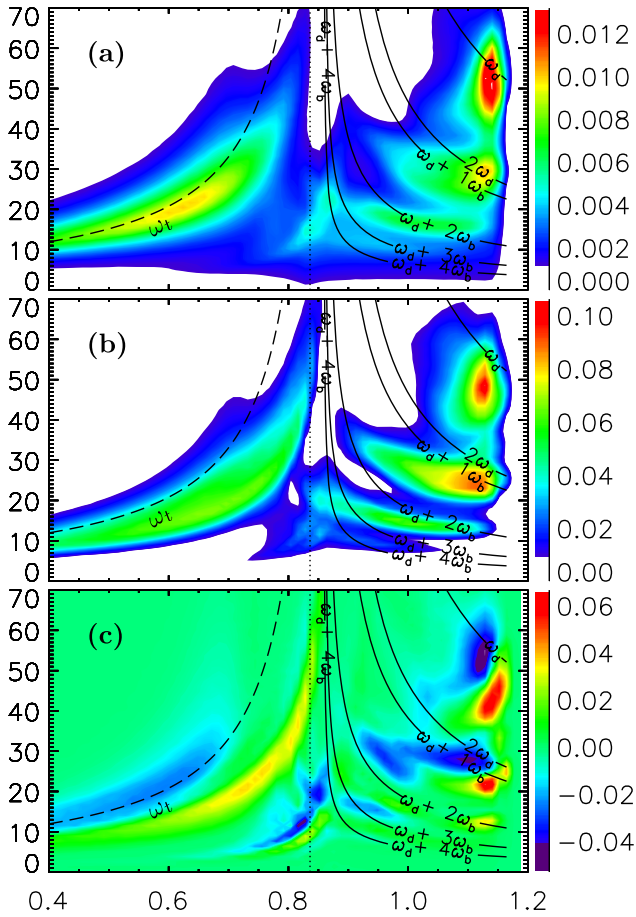

FIG. 4. Phase space (E, λ) structures of δf_h^2 at linear (panel a) and nonlinear (panel b) stages, and δf_h at nonlinear stages (panel c). Panel (a) is taken at time "A" in Fig. 1 of Ref. 50. Panels (b) and (c) are taken at time "C" in Fig. 1 of Ref. 50. Dotted line is the trapped-passing boundary. Solid and dashed lines are resonances for trapped and passing particles, respectively. The bounce frequency and precessional frequency are calculated according to Ref. 55.

nonlinear oscillation period of the wave frequency and amplitude. This linear phase-mixing time is typically shorter than the Coulomb collision or turbulence scattering time, which increases with the particle kinetic energy.[59] The destruction of the nonlinear islands by the linear free streaming is intrinsically a 2D process, which is beyond the 1D paradigm of Landau damping.[53]

Since P_ζ is related to the particle's radial position r and energy E, we further investigate the dynamics of the resonant particles in (r, ζ) and (E, ζ) phase space to delineate the contributions of the real space and velocity space in determining nonlinear BAE chirping dynamics (Fig. 5). We can see that the resonant islands width in real space is almost the same as the BAE mode width. The variation of r can easily induce 15% of the frequency chirping since $\omega_d \propto E/r$, while the energy variation of the resonant particle is about 4%. Therefore, we conclude that the frequency chirping of the BAE is mainly induced by the motion of the resonant particles in real space. Meanwhile, we can also see that the phase space structure in Fig. 5(a) is almost like the inverse structure of Fig. 5(b). This further confirms that the particle's radial position r is correlated with its kinetic energy E due to the constraint of the longitudinal invariant,[60] i.e., the outward (inward) moving particles in radial position r would decrease (increase) their kinetic energy E at the same time.

IV. WEAKLY DRIVEN BAE

After showing the saturation amplitude as a function of deviation from marginality and investigating the strongly
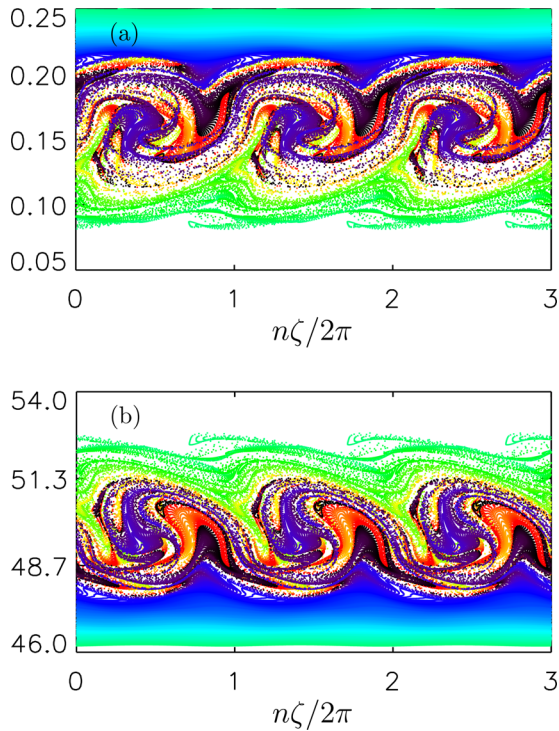
driven BAE simulation, we now reduce the EP density gradient to be $R_0/L_n = 20$ and excite the BAE again to investigate the nonlinear BAE behavior close to the marginality. The linear BAE frequency and damping rate are $\omega_{BAE} = 1.02\omega_0$ and $\gamma = 0.031\omega_0$, respectively. The small linear growth rate suggests that this is a weakly driven case. The linear BAE frequency is slightly higher than the strongly driven case due to the change of EP density gradient.[49] Figure 6(a) shows the time evolution of the ($n = 3$ and $m = 6$) mode at the mode rational surface. This mode reaches an oscillatory state after it saturates. The saturation amplitude $e\delta\phi/T \approx 0.022$ is much lower and the nonlinear oscillation period is shorter than the strongly driven case. The oscillation in one period is symmetry compared with the nonlinear oscillation in Fig.1(a) of Ref. 50. The frequency spectrum in Fig. 6(b) shows that the frequency chirping is much weaker. The time evolution of the dominant BAE frequency in Fig. 6(a) shows that there is no phase difference between the frequency and amplitude oscillation, which is different from the strongly driven results. The small frequency and amplitude oscillation range suggests that the weakly driven BAE is quite close to the steady state. The transition from the repetitive downward chirping state to the nearly steady state is also observed in recent BAE experiment in ASDEX,[21] which demonstrates qualitative agreement between the experiment and our nonlinear gyrokinetic simulation. Moreover, the different nonlinear BAE behaviors suggest that the nonlinear saturation mechanism is different between the strongly driven and weakly driven cases.

We further examine the poloidal mode structure of the weakly driven simulation. The linear mode structures are almost the same as the strongly driven case. However, the nonlinear mode structures are different when BAE amplitude decreases to the minimum. In the strongly driven simulation, the mode structure splits when the amplitude drops to the minimum (Fig. 7(a)). This is correlated with the frequency splitting in Fig. 1(b) of Ref. 50. There is no mode structure splitting in the weakly driven simulation when the BAE
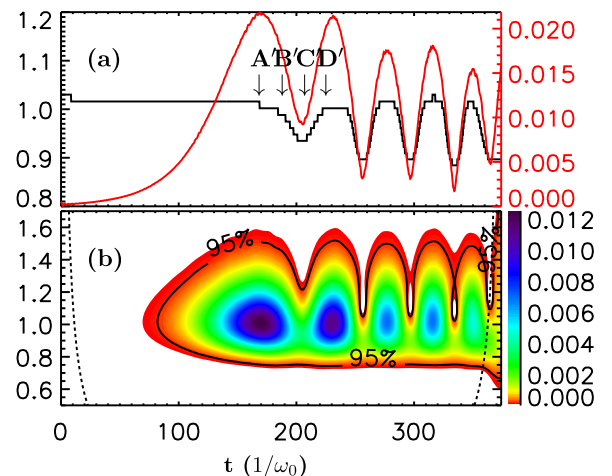

FIG. 5. The structure of the distribution function in (r, ζ) (a) and (E, ζ) (b) phase space at $t = 142/\omega_0$. The "Y" axis is r/a in panel (a) and E/T_i in panel (b). These particles are uniformly initialized in (ψ, ζ) plane with $\theta = 0$, $v_\parallel = 0.01\sqrt{T_i/m_i}$ and $\mu = 49T_i/B(r_0)$. The color represents the particles' initial P_ζ, which in the range of $[0.05, 0.59]\psi_w$. We can see from Fig. 4 that these particles are well located in the precessional resonance region.

FIG. 6. Time evolution of (a) BAE amplitude $e\phi/T_i$ (red) and dominant frequency ω (black), and (b) frequency power spectrum. The y-axis on the left is ω/ω_0. The unit of the power intensity in panel (b) is arbitrary.
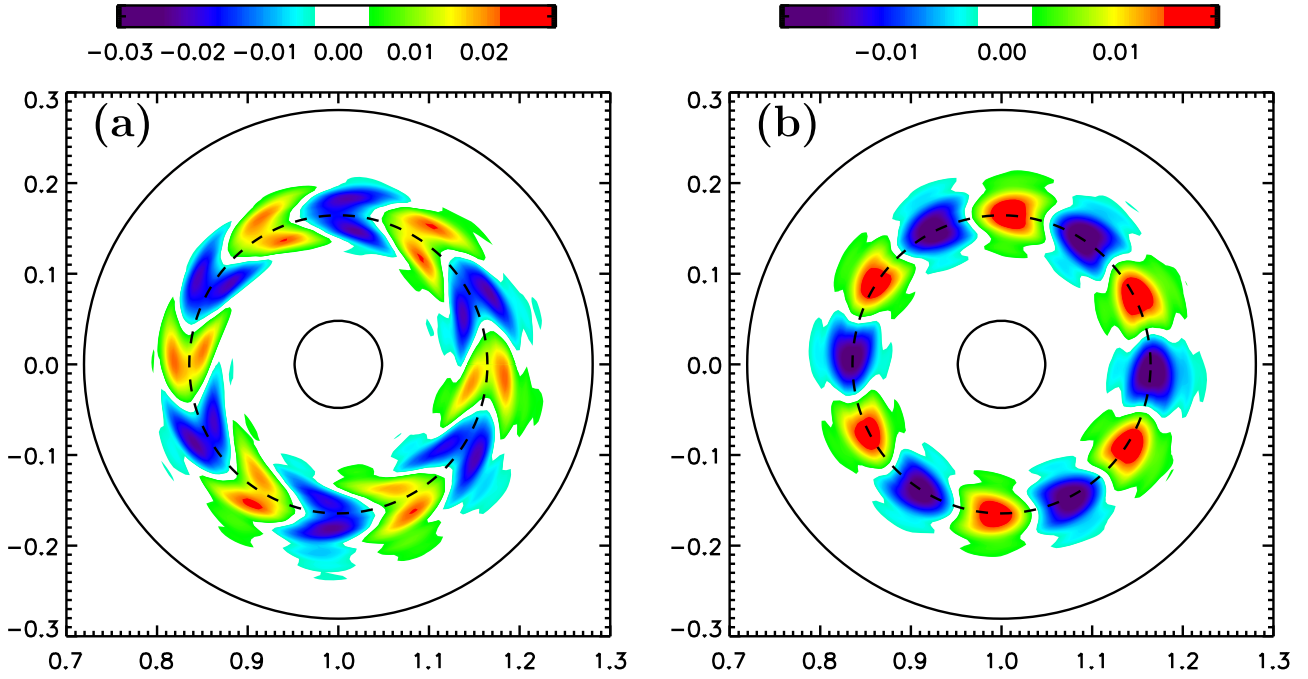
FIG. 7. The nonlinear poloidal mode structures when BAE amplitude decreases to the minimum for the strongly driven (a) and weakly driven (b) cases, respectively.

amplitude drops to the minimum. Some fine scale structures also appear in the radial direction.

In the weakly driven case, simulation with nonlinear thermal ions and linear EPs saturates at a high level, while simulation with linear thermal ions and nonlinear EPs has very similar nonlinear evolution compared with simulation with both nonlinearities (Fig. 8). Therefore, the EP nonlinearity dominates the nonlinear saturation, and the thermal ion nonlinearity plays little role for current simulation parameters. This result is quite different from the BAE simulation result in Sec. III, where the thermal ion nonlinearity plays an important role in determining the saturation level. The EP nonlinearity dominates the nonlinear BAE evolution for the weakly driven BAE, while thermal ion nonlinearity determines the saturation level in strongly driven BAE simulation. Therefore, nonlinear steady state in the weakly driven case and bursting state in the strongly driven case are determined by different nonlinear physics. Similar results are also

found in recent nonlinear TAE simulation,[54] where no significant difference was found between the results of the linear MHD and the nonlinear MHD simulations when saturation level is low, while the saturation level in the nonlinear MHD simulation is reduced to half compared to the linear MHD simulation when saturation level is high.

The linear EP entropy δf_h^2 of the weakly driven simulation is presented in Fig. 9. This structure is quite similar to the strongly driven results in Fig. 4. However, the resonant structures are narrower than that in the strongly driven case and the $p = 1$ drift-precessional resonance is well separated from the second harmonic resonance ($\omega = 2\omega_d$). The nonlinear δf_h^2 is almost the same as the linear structure in Fig. 4, and there is no downward shift of the resonance region because the nonlinear BAE has a much smaller frequency chirping range.

The evolution of $\delta f_h/f_{h0}$ in the (ζ, ω_d) phase space for the weakly driven simulation is shown in Fig. 10 in the linear wave frame. The linear phase space structures in Fig. 10(a) are quite similar to the linear structures of the strongly driven
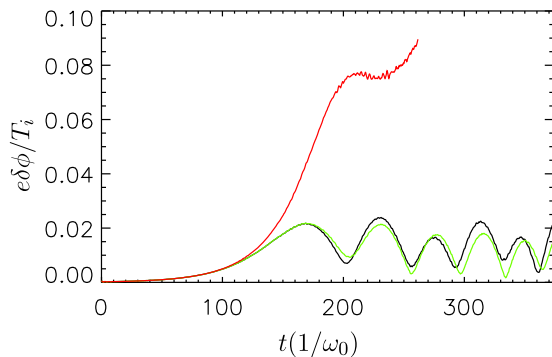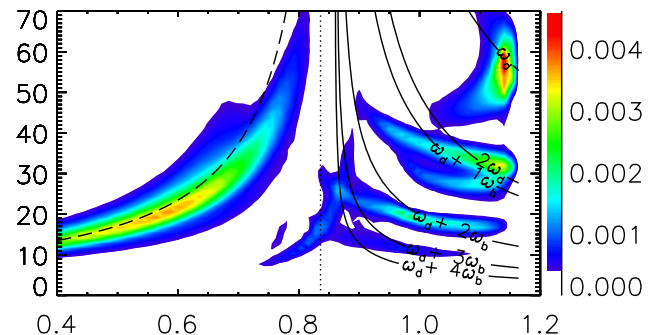

FIG. 8. Controlled simulations for weakly driven cases. Black line is the simulation with linear thermal ions and nonlinear EPs. Red line is the simulations with nonlinear thermal ions and linear EPs. Green line is the simulations with both nonlinearity.

FIG. 9. Linear phase space (E, λ) structures of δf_h^2 for weakly driven simulation.
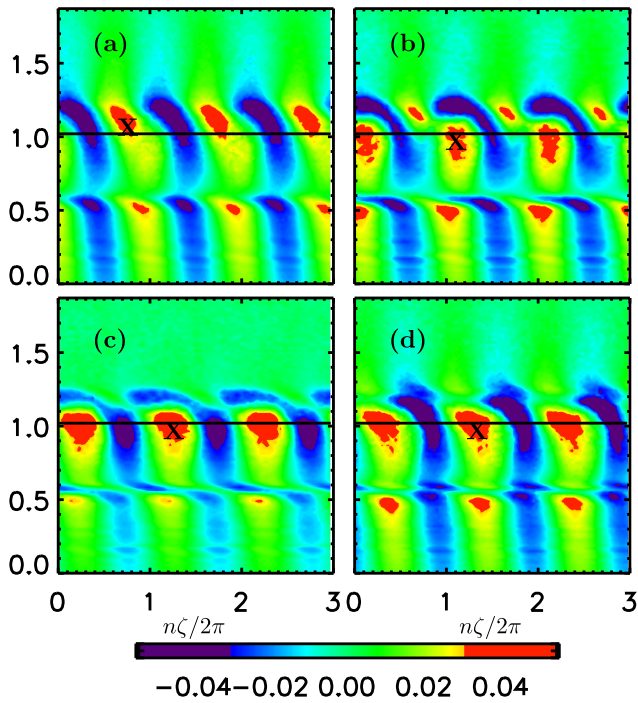
FIG. 10. Evolution of perturbed distribution function $\delta f_h/f_{h0}$ in (ζ, ω_d) phase space for the weakly driven simulation. The y-axis is ω_d/ω_0. Time steps (a)-(d) are $t = 168, 187, 206, 225$, which are labeled by A' − D' in Fig. 6. The trapped particles in the space of $r \in [0.14, 0.19]$ and $\theta \in [-0.25\pi, 0.25\pi]$ are taken into account.

FIG. 11. Evolution of distribution function in (ζ, P_ζ) space. Particle color represents initial P_ζ (normalized by $-\psi_w$). Dashed line represents the mode rational surface. The evolution of an island is tracked by "X." Time steps (a)-(d) are $t = 168, 187, 206, 225$, which are labeled by A' − D' in Fig. 6. These particles are initialized the same as those in Fig. 5 but with $\mu = 52T_i/B(r_0)$.

case in Fig. 3(a) of Ref. 50, and the second harmonic resonance $2\omega_d = \omega_{BAE}$ is more significant for the weakly driven case. When the mode saturates and the amplitude decreases, the dominant coherent structures (around the black line) are distorted into two layers in the ω_d direction. Each layer moves with its own local velocity, i.e., the upper layer moves to the negative ζ-direction due to its higher velocity and the lower layer moves to the positive ζ-direction. Therefore, the phase-mixing like structures are formed (Fig. 10(b)). When the BAE amplitude drops to the minimum (Fig. 10(c)), the upper layer is further phase-mixed and the related strength becomes weaker compared to the lower layer. This is correlated with the fact that the mode frequency also chirps to the minimum. When the upper layer shifts to the top of the nearby structures of the lower layer, the coherent structures evolve to the linear like structures and the BAE amplitude grows up again (Fig. 10(d)). Similar evolution of the coherent structures is also observed from the second harmonic resonance. These results clearly show that the nonlinear frequency and amplitude oscillation is due to the free streaming process of the coherent structures in phase space and this process repeats at the later nonlinear stage. The time it takes for the upper and lower layers move across one BAE wavelength is the linear phase-mixing time and is correlated with the period of the nonlinear BAE oscillation.

The (ζ, P_ζ) phase space structures of the weakly driven simulation are shown in Fig. 11. The linear phase space structure in Fig. 11(a) is quite similar to the linear structure in Fig. 4(a) of Ref. 50 except that the perturbation is dominantly located at the inner side of the $q = 2$ surface (lower side of P_ζ). The rotational structures are formed in Fig. 11(b) due to
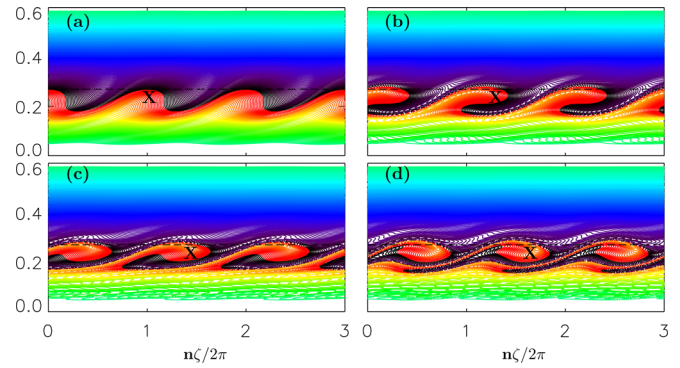
the wave-particle trapping and the BAE amplitude saturates. The resonant island width is smaller than the BAE mode width and is about half of the island width in Fig. 4(b) of Ref. 50 due to the small saturation amplitude in the weakly driven case. Therefore, the bounce period of the nonlinearly trapped particles in the weakly driven case is much longer than the bounce period in the strongly driven case. We further find that the saturation amplitude in the weakly driven simulation is about 20% of that in the strongly driven simulation, which is not proportional to the ratio of the island width between the weakly driven and strongly driven simulations. This result agrees with the scaling in Fig. 2, where the saturation amplitude is not proportional to the square of the linear growth rate for strongly driven simulation. When the linear drive is strong enough, the width of the resonant island is restricted by the BAE radial mode width due to the radial coordinate dependency of P_ζ. As the BAE amplitude decreases to the minimum, the red region and the blue region move across each other. Due to the variation of the radial BAE amplitude and the radial coordinate dependency of the precessional frequency, the resonance detuning occurs when the resonant particles move away from the resonant region, which is centered at the mode rational surface. The red region, which is around the rational surface, is completely convected back while the blue region, which is away from the rational surface, is dominated by the free streaming process, especially when the amplitude drops to the minimum. Therefore, the resonant particles around the rational surface (mostly the red region) are dominant by the wave-particle trapping while the particles away from the rational surface (the lower blue region) are dominant by free streaming. When the lower blue region moves to the bottom of the left island, the BAE grows up again (Fig. 11(d)). Since P_ζ approximately represents the radial position and the precessional frequency $\omega_d \propto E/r$, the free streaming of the lower P_ζ region is correlated with the free streaming of the higher ω_d layer in Fig. 10. We further find that the particle dynamics repeats in each nonlinear amplitude oscillation. These results clearly show that the nonlinear saturation and oscillation are due to the wave-particle trapping but the wave-particle trapping is much more complex than the conventional wave-particle trapping in 1D case.

Based on the conventional 1D paradigm, the wave-particle trapping period in the weakly driven case should be much longer than that in the strongly driven case. However, the nonlinear oscillation period in the weakly driven BAE is shorter than that in the strongly driven BAE. And there is a slow rotational motion around the rational surface (the red resonant region), which further indicates the nonlinear oscillation in the weakly driven BAE is not due to the conventional wave-particle trapping in the 1D case. The nonlinear BAE oscillation period is not correlated to the wave-particle trapping period, but correlated with the phase-mixing time, defined as the time it takes for the lower and upper resonant particles in P_ζ to move across each other in Fig. 11 or for the upper layer moves across one wave length in Fig. 10. These results emphasize the importance of the radial variation of the mode amplitude and the radial dependency of the "action" in the "action-angle" system for determining the nonlinear wave dynamics. The radial variation of the mode amplitude can allow free streaming and further modifies the wave-particle interaction especially when the mode amplitude drops to a low level.

V. PHASE SPACE STRUCTURE COMPARISON WITH THE 1D LANDAU DAMPING PROBLEM

In order to show the difference of the wave-particle interaction in the tokamaks from the conventional 1D nonlinear Landau damping problem,[53] we further carry out the 1D Landau damping simulation and investigate the resonant particle dynamics in (x, v) phase space. The conventional nonlinear theory shows that when wave amplitude is large enough, the resonant particles can be trapped and bounce inside the wave. The bounce period is correlated with the nonlinear amplitude oscillation period. The simplest case is the 1D electrostatic electron plasma oscillation (Fig. 12). In Fig. 12(a), the theoretical frequency is $\omega_r = 1.28\omega_{pe}$ for $k\lambda_D = 0.4$. Here, $\omega_{pe} = \sqrt{n_e e^2/m_e}$ and $\lambda_D = \sqrt{T_e/n_e e^2}$ are the Langmuir plasma frequency and Debye length, respectively. Thus, the resonant velocity is $v = \pm 3.2 v_e$, with $v_e = \sqrt{T_e/m_e}$. The wave frequency in our simulation agrees with the theory within 4%. Test particles are uniformly initialized in the (x, v) phase space with $v \in [-4, 36, -1.85]v_e$ so that only the $v < 0$ resonance is shown in the phase space. Figure 12(b) shows the nonlinear phase space structure at $t\omega_{pe} = 160$. The nonlinear resonant islands are well formed around the $v = -3.2 v_e$. The resonant particles are trapped by the wave and bounce inside the resonant islands, which induces the nonlinear amplitude oscillation, while the nonresonant particles are dominated by the free streaming process outside the resonant island. Since the mode amplitude variation only exists in x direction in the 1D simulation, the wave-particle trapping structure is well formed and the free streaming only occurs out of the resonant islands. It should be noted that the frequency oscillation is also observed in the nonlinear 1D O'Neil problem.[61] However, the wave growth rate is larger than the real frequency in Ref. 61. And the nonlinear amplitude oscillation frequency is comparable to the real frequency. Therefore, the dynamics of the frequency and amplitude in Ref. 61 is quite different from the 1D Landau damping simulation with a damping rate 5% of the real fre-
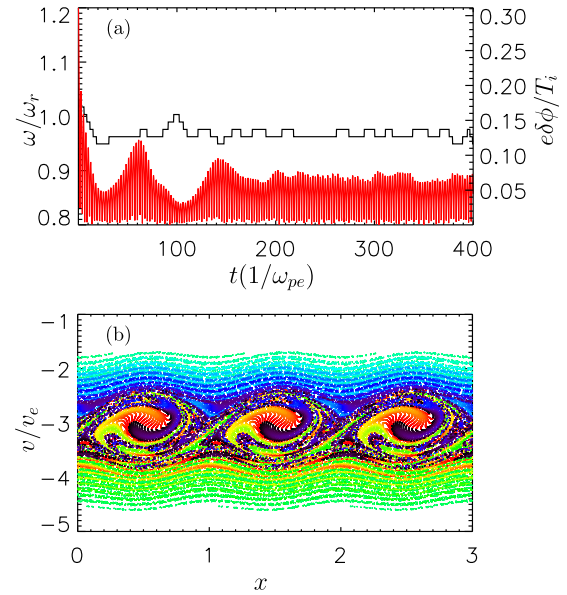

FIG. 12. Time evolution of the mode amplitude in the 1D Landau damping problem (a) and phase space structure in $x - v$ phase space (b). The resonant point in velocity space is $v = -3.2$.

quency, which is more comparable and relevant to the BAE case.

We also compare the resonant particle dynamics between the 1D Landau damping simulation, weakly driven and the strongly driven BAE simulations. The resonant particles are loaded in a single wave length with the color representing the initial "action" value (Fig. 13(a)). In the 1D Landau damping simulation (Fig. 13(b)), the nonlinear dynamics is mainly determined by the wave-particle trapping. The resonant particles are well trapped inside the single island, a small number of the resonant particles around the boundary of the island moves to the nearby islands due the variation of the maximum mode amplitude in each nonlinear oscillation. The nonresonant particles are slightly perturbed and are free streaming outside of the islands. In the weakly driven simulation (Fig. 13(c)), the wave-particle trapping period is much longer than the nonlinear oscillation period. Due to the radial variations of mode amplitude and radially asymmetric particle dynamics, the resonant particles of the upper P_ζ side (correspond to the lower velocity resonant particles) are well trapped and slowly rotate in the single wave length, while the resonant particles of the lower P_ζ side (correspond to the higher velocity resonant particles) are dominated by the free streaming process and part of them move to the nearby islands. The nonlinear oscillation period is correlated with the phase-mixing time. Therefore, the resonant particles cannot finish one bounce motion in a nonlinear oscillation period. In the strongly driven simulation (Fig. 13(d)), the width of the resonant islands is comparable to the BAE mode width. The bounce period, which is determined by the BAE mode width, is much faster than the weakly driven case and comparable to the phase-mixing time. All the resonant particles in the islands have some chance to free stream to the nearby islands due to the fast bounce motion. Meanwhile, the islands can be stretched into fragment structures through the free streaming process when the nonlinear BAE amplitude decreases to a
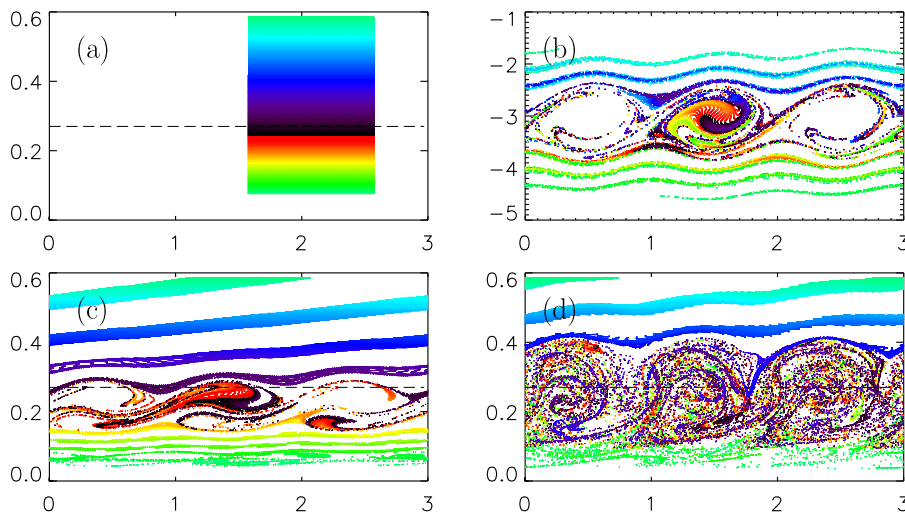
FIG. 13. Phase space structure comparison between the 1D Landau damping (b), the weakly driven BAE (c) and the strongly driven BAE (d) simulation. Panel (a) shows the particle are uniformly initialized in a single wave length with color represents the initial "action." Panels (a), (c), and (d) are plotted in (ζ, P_ζ) phase space, panel (b) is plotted in the (x, v) phase space. The particles in panels (b), (c), and (d) are initialized the same as Figs. 5, 11, and 12 respectively.

small level (Fig. 4(d) of Ref. 50), which will further be distorted by the new islands and result in more complex structures. We can see that the resonant particles are almost equally distributed in the whole resonance region after a few nonlinear oscillations. Overall, the wave-particle interaction in the tokamak geometry is much more complex than the conventional 1D Landau damping case.

VI. CONCLUSION

In this work, the gyrokinetic particle simulations are carried out to study the nonlinear BAE in toroidal plasmas. We find that the BAE saturation amplitude depends linearly on the square of the linear growth rate near marginality, while has no clear dependence on the linear growth rate when the BAE is well deviated from the marginality. In the strongly driven case, the nonlinear BAE exhibits a bursting state with fast and repetitive downward chirping. The chirping has a period of sub-millisecond and has a 90° phase ahead of the amplitude oscillation. The thermal ion nonlinearity plays a dominant role in determine the nonlinear saturation. In the weakly driven case, the nonlinear BAE exhibits a nearly steady state. The frequency chirping is small and has no phase difference compared to the amplitude oscillation. The nonlinear dynamics is determined by the energetic particle nonlinearity. We further find that the nonlinear BAE oscillation and frequency chirping are correlated with the evolution of the energetic particles in phase space for both the strongly and weakly driven cases. By comparison of the phase space structures between the nonlinear BAE and the one-dimensional nonlinear Landau damping, it is found that the wave-particle interaction in the toroidal geometry is much more complex than the conventional one-dimensional wave-particle interaction paradigm due to the radial variation of mode amplitude and the radially asymmetric guiding center dynamics.

ACKNOWLEDGMENTS

[1]W. W. Heidbrink, E. J. Strait, M. S. Chu, and A. D. Turnbull, Phys. Rev. Lett. **71**, 855 (1993).
[2]W. W. Heidbrink, E. Ruskov, E. M. Carolipio, J. Fang, M. A. Van Zeeland, and R. A. James, Phys. Plasmas **6**, 1147 (1999).
[3]A. D. Turnbull, E. J. Strait, W. W. Heidbrink, M. S. Chu, H. H. Duong, J. M. Greene, L. L. Lao, T. S. Taylor, and S. J. Thompson, Phys. Fluids B **5**, 2546 (1993).
[4]M. S. Chu, J. M. Greene, L. L. Lao, A. D. Turnbull, and M. S. Chance, Phys. Fluids B **4**, 3713 (1992).
[5]N. Winsor, J. L. Johnson, and J. M. Dawson, Phys. Fluids **11**, 2448 (1968).
[6]F. Zonca, L. Chen, and R. Santoro, Plasma Phys. Controlled Fusion **38**, 2011 (1996).
[7]B. N. Breizman, M. S. Pekker, S. E. Sharapov, and JET-EFDA Contributors, Phys. Plasmas **12**, 112506 (2005).
[8]R. Sabot, A. Macor, C. Nguyen, J. Decker, D. Elbeze, L.-G. Eriksson, X. Garbet, M. Goniche, G. Huysmans, Y. Ladroit, P. Maget, and J. L. Segui, Nucl. Fusion **49**, 085033 (2009).
[9]Z. O. Guimaraes-Filho *et al.*, Plasma Phys. Controlled Fusion **53**, 074012 (2011).
[10]M. Garcia-Munoz *et al.*, Phys. Rev. Lett. **100**, 055005 (2008).
[11]A. G. Elfimov *et al.*, Plasma Phys. Controlled Fusion **53**, 025006 (2011).
[12]W. Chen *et al.*, Nucl. Fusion **51**, 063010 (2011).
[13]W. Chen *et al.*, Phys. Rev. Lett. **105**, 185004 (2010).
[14]W. W. Heidbrink, Plasma Phys. Controlled Fusion **37**, 937 (1995).
[15]M. Podesta, R. E. Bell, N. A. Crocker, E. D. Fredrickson, N. N. Gorelenkov, W. W. Heidbrink, S. Kubota, B. P. LeBlanc, and H. Yuh, Nucl. Fusion **51**, 063035 (2011).
[16]M. Podesta, R. E. Bell, A. Bortolon, N. A. Crocker, D. S. Darrow, A. Diallo, E. D. Fredrickson, G.-Y. Fu, N. N. Gorelenkov, W. W. Heidbrink, G. J. Kramer, S. Kubota, B. P. LeBlanc, S. S. Medley, and H. Yuh, Nucl. Fusion **52**, 094001 (2012).
[17]G. J. Kramer *et al.*, Phys. Rev. Lett. **83**, 2961 (1999).
[18]R. F. Heeter, A. F. Fasoli, and S. E. Sharapov, Phys. Rev. Lett. **85**, 3177 (2000).
[19]M. P. Gryaznevich and S. E. Sharapov, Nucl. Fusion **46**, S942 (2006).
[20]W. Chen, J. Xiaoquan, Y. Qingwei, D. Xuantong, L. Yi, F. Beibin, H. Yuang, L. Wei, Z. Yan, Z. Jun, S. Xianming, L. Liancai, D. Xuru, and HL-2A Team, J. Phys. Soc. Jpn. **79**, 044501 (2010).
[21]I. G. J. Classen *et al.*, Plasma Phys. Controlled Fusion **53**, 124018 (2011).
[22]Ph. Lauber, I. G. J. Classen, D. Curran, V. Igochine, B. Geiger, S. da Graca, M. Garcia-Munoz, M. Maraschek, P. McCarthy, and ASDEX Upgrade Team, Nucl. Fusion **52**, 094007 (2012).
[23]P. Lauber, M. Brudgam, D. Curran, V. Igochine, K. Sassenberg, S. Gunter, M. Maraschek, M. Garcia-Munoz, N. Hicks, and ASDEX Upgrade Team, Plasma Phys. Controlled Fusion **51**, 124009 (2009).
[24]A. Bondeson and M. S. Chu, Phys. Plasmas **3**, 3013 (1996).

[25]C. Nguyen, X. Garbet, and A. I. Smolyakov, Phys. Plasmas **15**, 112502 (2008).

[26]A. I. Smolyakov, C. Nguyen, and X. Garbet, Nucl. Fusion **50**, 054002 (2010).

[27]C. Nguyen, X. Garbet, R. Sabot, L.-G. Eriksson, M. Goniche, P. Maget, V. Basiuk, J. Decker, D. Elbeze, G. T. A. Huysmans, A. Macor, J.-L. Segui, and M. Schneider, Plasma Phys. Controlled Fusion **51**, 095002 (2009).

[28]C. Nguyen, X. Garbet, V. Grandgirard, J. Decker, Z. Guimaraes-Filho, M. Lesur, H. Lutjens, A. Merle, and R. Sabot, Plasma Phys. Controlled Fusion **52**, 124034 (2010).

[29]H. L. Berk and B. N. Breizman, Phys. Fluids B **2**, 2226 (1990).

[30]H. L. Berk, B. N. Breizman, and N. V. Petviashvili, Phys. Lett. A **238**, 408 (1998).

[31]H. L. Berk, B. N. Breizman, and N. V. Petviashvili, Phys. Lett. A **234**, 213 (1997).

[32]H. L. Berk, B. N. Breizman, J. Candy, M. Pekker, and N. V. Petviashvili, Phys. Plasmas **6**, 3102 (1999).

[33]R. G. L. Vann, H. L. Berk, and A. R. Soto-Chavez, Phys. Rev. Lett. **99**, 025003 (2007).

[34]M. K. Lilley, B. N. Breizman, and S. E. Sharapov, Phys. Plasmas **17**, 092305 (2010).

[35]S. D. Pinches, H. L. Berk, M. P. Gryaznevich, S. E. Sharapov, and JET-EFDA Contributors, Plasma Phys. Controlled Fusion **46**, S47 (2004).

[36]G. Y. Fu *et al*., Phys. Plasmas **13**, 052517 (2006).

[37]J. Y. Lang, G. Y. Fu, and Y. Chen, Phys. Plasmas **17**, 042309 (2010).

[38]F. Zonca, S. Briguglio, L. Chen, G. Fogaccia, and G. Vlad, Nucl. Fusion **45**, 477 (2005).

[39]X. Wang, F. Zonca, and L. Chen, Plasma Phys. Controlled Fusion **52**, 115005 (2010).

[40]X. Wang, F. Zonca, and L. Chen, "Nonlinear dynamics of beta induced Alfvén eigenmode driven by energetic particles," Phys. Rev. E **86**, 045401 (2012).

[41]Z. Lin, T. S. Hahm, W. W. Lee, W. M. Tang, and R. B. White, Science **281**, 1835 (1998).

[42]Y. Nishimura, Phys. Plasmas **16**, 030702 (2009).

[43]W. L. Zhang, I. Holod, Z. Lin, and Y. Xiao, Phys. Plasmas **19**, 022507 (2012).

[44]W. J. Deng, Z. Lin, I. Holod, X. Wang, Y. Xiao, and W. L. Zhang, Phys. Plasmas **17**, 112504 (2010).

[45]W. J. Deng, Z. Lin, I. Holod, X. Wang, Y. Xiao, and H. S. Zhang, Nucl. Fusion **52**, 043006 (2012).

[46]D. A. Spong, E. M. Bass, W. Deng, W. W. Heidbrink, Z. Lin, B. Tobias, M. A. Van Zeeland, M. E. Austin, C. W. Domier, and N. C. Luhmann, Jr., Phys. Plasmas **19**, 082511 (2012).

[47]H. S. Zhang, Z. Qiu, L. Chen, and Z. Lin, Nucl. Fusion **49**, 125009 (2009).

[48]H. S. Zhang and Z. Lin, Phys. Plasmas **17**, 072502 (2010).

[49]H. S. Zhang, Z. Lin, I. Holod, X. Wang, Y. Xiao, and W. L. Zhang, Phys. Plasmas **17**, 112505 (2010).

[50]H. S. Zhang, Z. Lin, and I. Holod, Phys. Rev. Lett. **109**, 025001 (2012).

[51]A. J. Brizard and T. S. Hahm, Rev. Mod. Phys. **79**, 421 (2007).

[52]I. Holod, W. L. Zhang, Y. Xiao, and Z. Lin, Phys. Plasmas **16**, 122307 (2009).

[53]T. M. O'Neil, Phys. Fluids **8**, 2255 (1965).

[54]Y. Todo, H. L. Berk, and B. N. Breizman, Nucl. Fusion **52**, 033003 (2012).

[55]Y. Q. Liu, M. S. Chu, C. G. Gimblett, and R. J. Hastie, Phys. Plasmas **15**, 092505 (2008).

[56]L. Chen, J. Geophys. Res. **104**, 2421, doi:10.1029/1998JA900051 (1999).

[57]R. B. White, *The Theory of Toroidally Confined Plasmas* (Imperial College Press, London, 2006).

[58]B. N. Breizman and S. E. Sharapov, Plasma Phys. Controlled Fusion **53**, 054001 (2011).

[59]W. L. Zhang, Z. Lin, and L. Chen, Phys. Rev. Lett. **101**, 095001 (2008).

[60]Y. Xiao and Z. Lin, Phys. Plasmas **18**, 110703 (2011).

[61]T. M. O'Neil, J. H. Winfrey, and J. H. Malmberg, Phys. Fluids **14**, 1204 (1971).